Acta Crystallographica Section B
Structural Science
ISSN 0108-7681

The structure of orange HgI_2. I. Polytypic layer structure

Marc Hostettler,* Henrik Birkedal† and Dieter Schwarzenbach

Institute of Crystallography, BSP Dorigny, University of Lausanne, CH-1015 Lausanne, Switzerland

† Present address: Department of Chemistry and Biochemistry, University of California, Santa Barbara, CA 93106-9510, USA.

Correspondence e-mail: marc.hostettler@ic.unil.ch

Received 15 July 2002
Accepted 5 September 2002

The metastable orange crystals of HgI_2 comprise three different crystal structures, all of which are built from corner-linked Hg_4I_{10} supertetrahedra. Two of them are end members with the maximum degree of order (MDO) of a polytypic layer structure; the third shows a three-dimensional linkage. This paper presents the determination from X-ray diffraction data of the tetragonal polytypic structures and their stacking disorder. Diffraction patterns show sharp Bragg reflections and rods of diffuse intensity with pronounced maxima. In a first step, the diffuse intensity was neglected and all maxima were treated as Bragg reflections. The crystal was supposed to be a conglomerate of the two MDO structures diffracting independently, and their parameters and volume ratio were refined against the single data set. The geometries and anisotropic displacement parameters of the layers in the two structures are shown to be nearly identical. Layer contacts in the two stacking modes are identical. The structures are fractal complications of the stable red form of HgI_2. In a second step, the stacking disorder has been quantitatively analyzed with a Markov chain model. Two probabilities describing next-nearest-layer interactions were visually adjusted to observed intensity profiles extracted from image-plate detector data. Results consistently show that the crystal comprises nearly equal volumes of MDO structures with an average domain thickness of about 5 layers or 30 Å.

1. Introduction

Mercuric iodide, HgI_2, has been studied intensively for many years since the discovery of its optoelectronic properties (Bube, 1957). Single crystals of the red phase, stable at ambient conditions, are currently used as components in γ- and X-ray detectors (Sharma *et al.*, 1994; Piechotka, 1997; Steiner *et al.*, 1999; Schieber *et al.*, 2001). Besides this red phase, two additional phases, both metastable, are known at ambient conditions. One of them is yellow; the other shows various hues of orange. Both can be obtained by sublimation of red HgI_2. Kleber *et al.* (1968) carried out a systematic study of the crystallization of HgI_2 from the melt, by sublimation and by evaporation from 15 solvents. All three forms, red, yellow and orange, cocrystallize from organic solvents such as acetone or 2-chloroethanol in various ratios depending on the solvent. The structure of the red tetragonal phase (Bijvoet *et al.*, 1926; Jeffrey & Vlasse, 1967) consists of layers of corner-linked HgI_4 tetrahedra. The stacking of these layers results in a cubic closest packing of I atoms. Using yellow crystals grown by sublimation, Jeffrey & Vlasse (1967) showed this phase to be isostructural with $HgBr_2$. The structural motif is a linear I—Hg—I molecule. The yellow phase crystallized from solu-

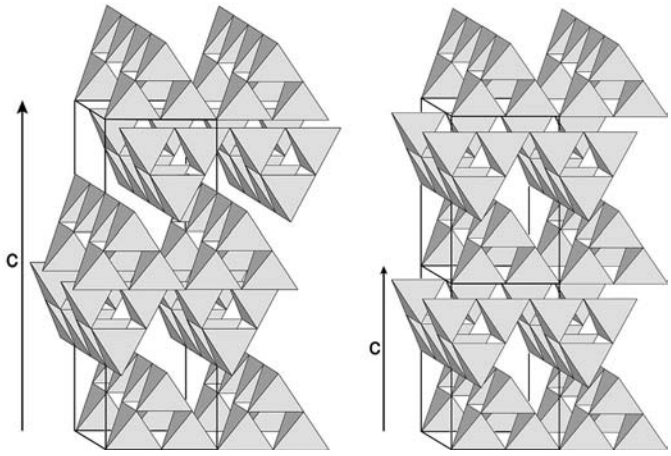

Figure 1
The idealized model of Schwarzenbach (1969). Left: the four-layer stacking ($I4_1/amd$). Right: the two-layer stacking ($P4_2/nmc$). I and Hg atoms are, respectively, at the corners and centers of the tetrahedra. The site symmetry of the supertetrahedra is $\bar{4}m2$. See also Fig. 5

tion possesses the same structure (Hostettler, 2002). On heating, the red and orange crystals transform into another yellow phase, which is stable above about 400 K and whose structure is not identical with that of the metastable yellow phase (Hostettler *et al.*, 2001).

Orange HgI_2 was first described by Kohlschütter (1927) who obtained morphologically tetragonal crystals with many faces from HgI_2 vapor. Gorskii used optical goniometry and the X-ray Laue technique in a very careful study of orange crystals with tetragonal or trigonal habitus grown from solution. He was not able to propose a structural model (Gorskii, 1934, 1935). The orange single crystals of Jeffrey & Vlasse (1967) were multiple-growth twins, as revealed by polarized light microscopy and X-ray diffraction. Structure determination was again unsuccessful. Schwarzenbach (1969), hereafter referred to as S69, observed rods of diffuse intensity on precession photographs and the presence of numerous systematic absences in excess of any possible space-group absences, suggesting a disordered polytypic layer structure. He derived an idealized structural model that reproduces the absences and an analytical expression for the diffuse scattering involving Markov-chain probabilities that allowed a qualitative comparison with experiment. The structural motif is an Hg_4I_{10} supertetrahedron formed by four corner-linked HgI_4 tetrahedra. The supertetrahedra are corner-linked into layers that may be regarded as fractal complications of the layers in red HgI_2. The stacking of these layers easily explains the polytypic disorder (Fig. 1). As in red HgI_2, I atoms are cubic closest packed. However, doubts have been formulated as to the correctness of this idealized structure (Vannerberg, 1970). Recently, the structures of $KGaTe_2$ and $KAlTe_2$ have been published (Kim & Hughbanks, 2000). The structure of these chalcogenides shows layers of corner-linked X_4Te_{10} (X = Ga, Al) supertetrahedra, similar to the idealized model of S69, the only difference being the presence of K ions between the layers. A review article on the Hg—I system (Gumiński, 1997) presents most of the results published to date on HgI_2.

In this contribution we present a redetermination, confirmation and quantitative refinement of the polytypic orange structure. In the companion paper (Hostettler & Schwarzenbach, 2002), we present a new structure belonging to the orange HgI_2 family of structures, showing Hg_4I_{10} supertetrahedra corner-linked into interpenetrating diamontoid frameworks, and a twinning model explaining the various previously published observations. The formalism used to describe the polytypic disorder is presented in §3.2

2. Experimental

2.1. Crystallization

Using the same method as S69, we have obtained all samples by evaporation of a solution of commercial HgI_2 powder (Fluka 83379) in 2-chloroethanol. Orange, yellow and red crystals grow within the same batch. The ratio of the number of crystals of the three polymorphs depends on the solvent (Kleber *et al.*, 1968), the temperature of the solution and the concentration. Heating the solution favors the formation of yellow crystals for any solvent. With 2-chloroethanol in particular, yellow crystals are obtained as the sole product at temperatures above 323 K. The speed of evaporation clearly governs the crystallization process. Yellow molecular HgI_2 crystallizes within a few hours, while the growth of the orange and red polymorphs takes several days and days to weeks, respectively. It appears that precipitation of yellow crystals, which are more unstable than red or orange crystals, can be favored by removing solvent rapidly. The phenomenon of concomitant polymorphs has recently been reviewed by Bernstein *et al.* (1999).

2.2. Stability of the crystals

Both the orange and yellow crystals are mechanically unstable. Contact with a needle, such as during an attempt to remove a crystal from a dish, most often induces the transformation to the red phase. However, the orange form is considerably more stable than the yellow form at ambient conditions. The conversion of the yellow crystals to the red phase takes only a few seconds. A red nucleus appears at the point of contact and grows rapidly through the entire crystal. The slower transformation of orange to red crystals takes a few hours. It starts with irregularly shaped red nuclei near the point of contact, which subsequently grow and merge. However, it is possible with care and patience to mount orange crystals on glass fibres without creating red nuclei. Generally, mounted crystals remain orange during the subsequent three or four days. In one exceptional case, an orange crystal did not transform for 12 months (sample 1, see below). At ambient pressure, the orange crystals are metastable between 100 K, the lowest temperature investigated, and 400 K. We were able to heat orange crystals to about 400 K where they transform to the yellow high-temperature phase. This observation contradicts Kleber *et al.* (1968) who observed an orange crystal transform into the red form at 333 K and concluded that the orange form could therefore not persist above this tempera-

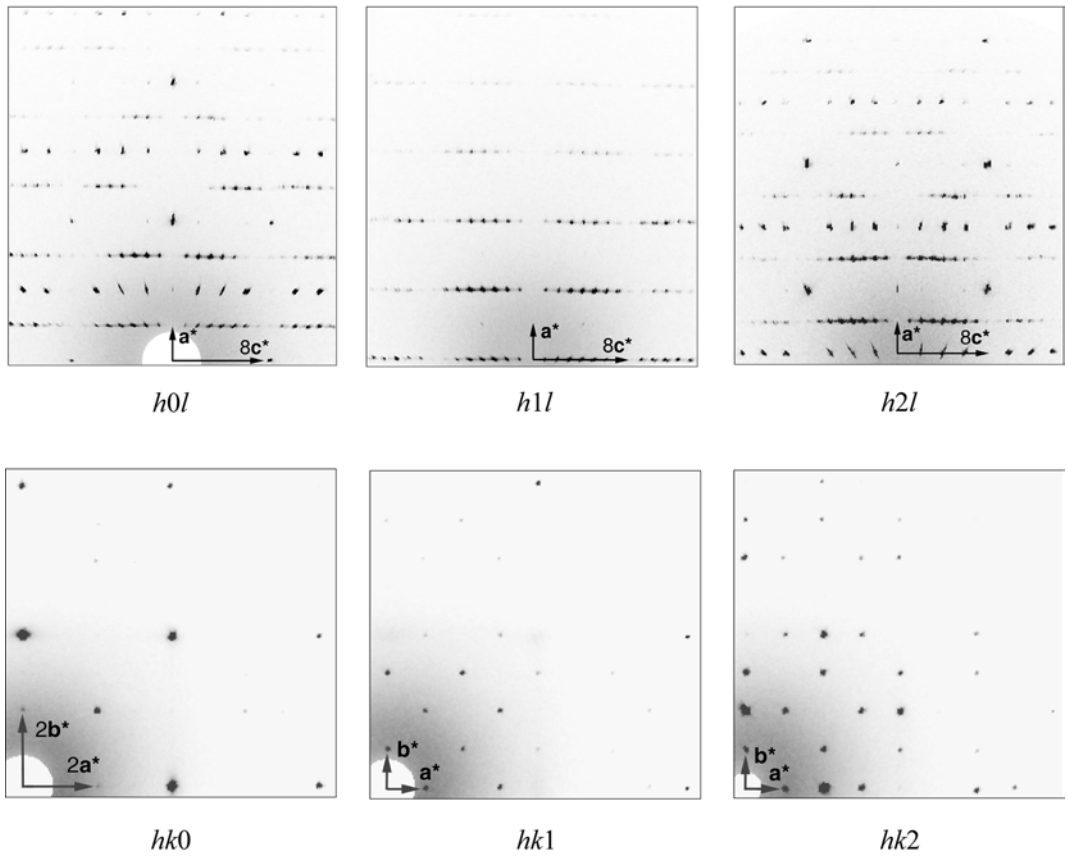

Figure 2
Reconstructed reciprocal layers of (1). The point-group symmetry of the diffraction patterns is 4/*mmm*.

ture. The sensitivity of the orange form to minor shocks may explain this finding.

After the transformation from orange to red, the resulting crystal quality is poor, as evidenced by broad Bragg reflections. Some orange crystals after exposure to X-rays do not convert to the red form but instead become colorless and transparent and lose their crystallinity. They appear to be amorphous and may be decomposition products. In one case, a three-month-old orange sample transformed into yet another orange phase with a more yellow hue and a different diffraction pattern (Hostettler & Schwarzenbach, 2002).

2.3. X-ray diffraction

Orange crystals were mounted on glass fibres. Grease (Apiezon, UK) was used instead of glue. Out of a large number of mounted fresh orange crystals, only four did not develop red nuclei after 1 h. Subsequent X-ray diffraction experiments on these crystals were carried out using several diffractometers equipped with area detectors and Mo $K\alpha$ radiation. Sample (1) showed the highest crystal quality as evidenced by relatively sharp diffraction spots and low s.u. values of the tetragonal lattice constants. It also showed rods of diffuse scattering parallel to c^* indicating a polytypic structure. It was used to collect a low-temperature intensity data set at 200 K on a KUMA diffractometer equipped with an Oxford Cryosystem, graphite-monochromated Mo $K\alpha$ radiation and a CCD detector. This data has been used for structure determination and refinement. Another data set from this crystal was collected at room temperature and used for the reconstruction of undistorted reciprocal space (Fig. 2). Crystal data and experimental parameters are given in Tables 1 and 2.[1] On lowering the temperature from 293 K to 200 K, the lattice constants change as would be expected for a layer structure: the dimensions of an individual layer defined by a hardly change while c, and thus the interlayer distance, contracts. The ratio c/a changes from 2.8119 (11) to 2.8074 (4).

Sample (2) was of inferior quality. The lattice constants obtained with different instruments have large s.u. values and poor reproducibility. This is due to pronounced arcing of the reflections. Some of them are smeared over arcs spanning angles of up to 20° (Fig. 3). Similar arcing has been observed for polytypic crystals of CdI_2 and has been ascribed to dislocations that form the boundaries between deformed mosaic grains (Trigunayat & Verma, 1962; Trigunayat, 1966). The orientation matrix of (2) could not be determined precisely enough to allow reliable integration over Bragg peaks. Sample (3) was twinned, and sample (4) showed an altogether different diffraction pattern (Hostettler & Schwarzenbach, 2002). The stability of the samples appears to be connected

[1] Supplementary data for this paper are available from the IUCr electronic archives (Reference: BK0119). Services for accessing these data are described at the back of the journal.

Table 1
Experimental details at 200 K.

Chemical Formula	HgI_2
Formula weight (g mol^{-1})	454.4
Crystal habit	Truncated pyramid
Laue symmetry	4/*mmm*
θ_{max} (°)	26.38
No. of measured, independent reflections	7851, 843
Average completeness (till 0.8 Å resolution)	98.4%
Average redundancy in point group 4/*mmm*	8.7
Range of *h*, *k*, *l*	$-10 \le h \le 10$ $-10 \le k \le 10$ $-26 \le l \le 30$
Radiation (Å)	Mo $K\alpha$, $\lambda = 0.71073$
μ (mm^{-1})	45.09
Transmission T_{min}, T_{max}	0.017, 0.411
R_{int} before, after absorption correction	0.2496, 0.0730

Computer programs used. Data reduction and structure solution: *KM4CCD* (Oxford Diffraction, 2001), *XSHAPE* (Stoe & Cie GmbH, 1997), *XPREP* (XPREP, 1996), *SHELXS* (Sheldrick, 1997) and home-written programs. Structure refinement: *STACK* (Birkedal *et al.*, 1998).

with the crystal quality: (2) and (3) converted to the red phase in less than a month, whereas (1) remained orange for a year.

2.4. Data reduction

The Bragg intensities of (1) at 200 K were extracted from the CCD images by integration over three-dimensional profile functions using the program *CrysAlis* (Oxford Diffraction, 2001). The program optimizes the profile function of each individual reflection using the $\sigma(I)/I$ method of Lehmann & Larsen (1974). The maxima located on rods of diffuse intensity were treated as if they were normal Bragg reflections. The intensities were then corrected for Lorentz and polarization (Lp) effects. Absorption was corrected analytically using the shape of the crystal measured with a high-resolution telescope. Undistorted layers of the reciprocal lattices (Figs. 2 and 3) were reconstructed from the image-plate exposures of (1) and (2) at room temperature, using the software of the Stoe image-plate diffractometer *IPDS* (Stoe & Cie GmbH, 1997).

Table 2
Crystal data and experimental details that differ at 200 K and room temperature.

	Temperature (K)	
	200 (1)	293 (1)
Diffractometer	Kuma CCD	Stoe IP
Data collection method	ω scan	φ scan
Oscillation steps (°)	0.3	1.0
Number of images	1484	348
Exposure time per image (s)	2 × 35	150
Total exposure time (h)	28	15
Total data collection time (h)	33	40
a (Å)	8.7863 (5)	8.7860 (9)
c (Å)	24.667 (3)	24.705 (9)
Volume (Å^3)	1904.3 (4)	1907.1 (11)
Data used for	Structure solution and refinement	Fig. 2, extraction of diffuse profiles

2.5. Extraction of the diffuse intensities

Intensity profiles along c^* have been extracted from the reconstructed layers using *IGOR* (2000). The procedure is depicted in Fig. 4. Rectangular boxes were chosen along three rods of diffuse intensities [(10*l*), (30*l*) and (41*l*)]. At each point *l* inside the box, the intensity was integrated from $k - 0.05$ to $k + 0.05$. These integration limits in *k* were chosen such that the intensities outside the boxes contained nothing but background intensity. The average background was calculated as the average of the two profiles integrated from $k - 0.15$ to $k - 0.05$ and $k + 0.05$ to $k + 0.15$, and this was subtracted from the intensity profiles. A polarization and an equatorial Lorenz correction have been applied. The absorption was corrected analytically by the interpolation of

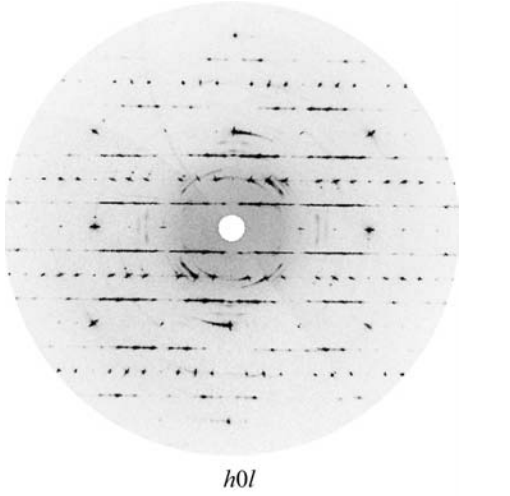

Figure 3
Reconstructed reciprocal layer of (2). In addition to the diffuse streaks already observed in the diffraction pattern of (1), the phenomenon of arcing is observed. The (400) reflection presents up to 20° of arcing. Note the poor crystal quality of this sample compared with (1).

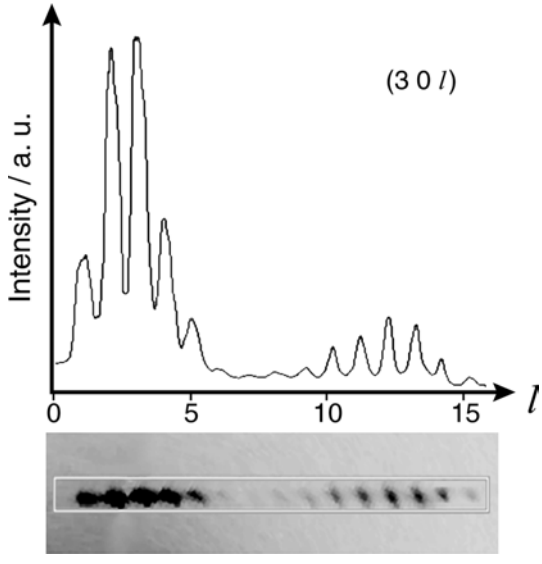

Figure 4
Extraction of intensity profiles from reconstructed layers of reciprocal space. Bottom: detail of the *h0l* layer. Top: the (30*l*) extracted intensity profile.

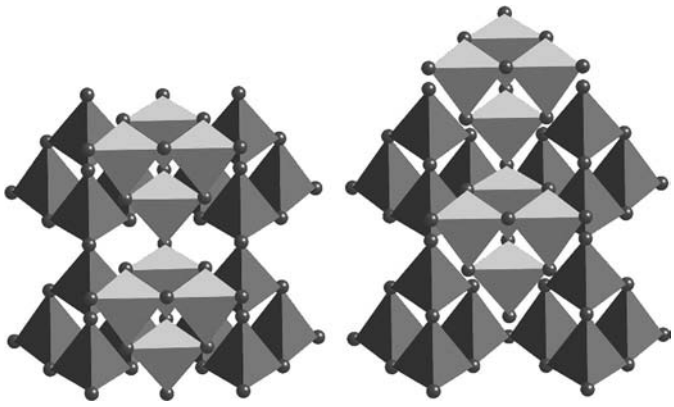

Figure 5
The two types of stacking of two layers, *f* stack (left) and *t* stack (right). The single layer has symmetry $p\bar{4}m2$. Corresponding MDOs are shown in Fig. 1.

the transmission factors calculated at each reciprocal lattice point.

3. Structure determination

3.1. Description of the diffraction pattern

The diffraction patterns of (1) (Fig. 2) show sharp Bragg reflections that can be indexed according to the tetragonal cell given in Table 2. There are numerous and very peculiar systematic absences, in excess of any possible space-group absences. Superimposed on some of the lattice rows parallel to c^* are rods of diffuse scattering. These observations are the hallmark of polytype disorder. S69 described red–orange and yellow–orange crystals. For the latter, the following conditions were reported for observed reflections h, k, l: if $h, k = 2n$ and $h + k = 4n$ then $l = 8n$; if $h, k = 2n$ and $h + k = 4n + 2$ then $l = 2n$ but not $8n$; if $h + k = 2n + 1$ then $l \neq 8n$; there are no observed reflections if $h, k = 2n + 1$. Rods of diffuse intensity were observed for $h + k = 2n + 1$. Except for the decrease as a function of $\sin\theta/\lambda$ due to the decrease of the scattering factor of Hg, the diffuse intensity was described as periodic in l with period 8, and this was the same for all rods. The red–orange crystals showed the additional condition $h + k = 2n + 1$, $l = 2n + 1$, and no discernable diffuse intensities were reported. The diffraction patterns of (1) (Fig. 2) approximately agree with this description of the yellow–orange crystals for the complete reciprocal space to the experimental resolution of 0.8 Å, with two important differences. Some of the previously unobserved reflections are weakly observed, *e.g.* 108, 308, 218, 418, 402, 420, 820. By lowering the high tension on the X-ray tube, we found that the weak reflections 114 and 200 in Fig. 2 are due to $\lambda/2$ radiation. Also, different diffuse rods show different intensity variations. These observations indicate important deviations from the highly idealized structure proposed by S69.

The layer stacking in (2) appears to be more disordered than that in (1), as indicated by the rather intense diffuse rods $10l$ and $30l$ and the superimposed broad intensity maxima (Fig. 3). As in Fig. 2, there are some reflections that violate the reflection conditions of S69 (again, some are due to $\lambda/2$ radiation, *e.g.* 004). There are also spots, which may derive from differently oriented material, and intensities smeared out along arcs of up to 20°, as mentioned above. Thus, (2) is similar to (1) but of inferior quality.

3.2. Polytypic disorder

Polytypic disorder is generally due to the existence of alternative relative positions of two neighboring layers showing the same or very similar interlayer contacts. In polytypic orange HgI_2 in particular, successive layers may assume the two relative positions shown in Fig. 5, which we designate by *f* and *t*. Every member of the polytypic family of structures is described by a succession of the letters *f* and *t*. The simplest end members are the structures with maximum degree of order (MDO) (Dornberger-Schiff, 1979), defined by a single type of stacking: all *f* (MDO1) or all *t* (MDO2). Space groups are $I4_1/amd$ for MDO1 and $P4_2/nmc$ for MDO2. The *c* translations of MDO1 and MDO2 comprise four and two layers, respectively, whereas *a* is identical for both structures. The intensity maxima situated on the diffuse rods ($h + k = 2n + 1$) of (1) are quite sharp. As proposed by S69, the crystal may be described in good approximation as a conglomerate of the structures MDO1 and MDO2. Neglecting the diffuse intensities and accepting all reflections as Bragg reflections, we obtain a model consisting of two coexisting structures possessing the same tetragonal unit cell (Table 2): for MDO1, this is the conventional unit cell, whereas *c* of the conventional unit cell of MDO2 is doubled. Table 3 classifies the reflections of the data set into groups belonging, respectively, to MDO1 only, to MDO2 only and to both structures.

3.3. Average structure

S69 derived the structure of the orange phase from the fact that the *hk*0 and *hhl* reciprocal lattice planes are very similar to the *hk*0 plane of the red phase. In the present work, we applied direct methods including all reflections and assuming space group $I4_1/amd$. The resulting structure is thus expected to be an average of the two MDO structures with disordered Hg atoms. This is close to an equi-atom structure, as the diffracting powers of an I atom and of half a Hg atom are similar (53 and 40 electrons, respectively). Of the five atoms in the asymmetric unit, four were found automatically. Three of these were close to the positions of a cubic closest packing and were therefore assumed to be I atoms. The positions of the Hg atoms were then easily found from a Fourier map. The resulting structure is interpreted as a superposition of two stacking sequences of layers of corner-linked Hg_4I_{10} supertetrahedra and may be decomposed into the two MDO structures proposed by S69.

3.4. Refinement of the conglomerate of MDO structures

The parameters of the two independent structures MDO1 and MDO2 and their volume ratio have been refined against a single data set. Assuming that the domains are sufficiently

Table 3
Reflections arising from domains with maximum degree of order: MDO1 only (symmetry $I4_1/amd$), MDO2 only (symmetry $P4_2/nmc$ referred to a cell with double c axis) and both domains.

Number of unique reflections in parentheses. Diffuse rods run through reflections with $h + k = 2n + 1$. S69 reported additional non-space-group absences, most but not all of which have zero intensities in the present work (see text). In particular, reflections with both h and k odd have never been observed.

Class	MDO1 (273)	MDO2 (258)	Both (312)	Space group absent
hkl	$h + k = 2n + 1$, $l = 2n + 1$	$h + k = 2n + 1$, $l = 2n$	$h + k = 2n$, $l = 2n$	$h + k = 2n$, $l = 2n + 1$
*hk*0		$h = 2n + 1$, $k = 2n + 1$	$h = 2n$, $k = 2n$	$h + k = 2n + 1$
0*kl*	$(k = 2n + 1, l = 2n + 1)$	$(k = 2n + 1, l = 2n)$	$(k = 2n, l = 2n)$	$(k = 2n, l = 2n + 1)$
hhl	$h = 2n + 1$, $l = 4n + 2$	$h = 2n + 1$, $l = 4n$	$h = 2n$, $l = 4n$	$h = 2n$, $l = 4n + 2$ (or $2n + 1$)

Table 4
Refinement with program *STACK*, reliability factors, 40 refined parameters.

The refined volume fractions are $v_1 = 0595\,(13)$ and $v_2 = 0405\,(6)$ for MDO1 and MDO2, respectively. Reflections are classed as common to both structures and arising from one structure only.

	All	MDO1 + MDO2	MDO1 only	MDO2 only
No. of reflections	843	312	273	258
$R_1(I/\sigma>3)$	0.066	0.064	0.068	0.069
wR_2	0.134	0.130	0.135	0.143
S(all)	1.066			

large to diffract like independent crystals and that interference terms are negligible, the squared structure amplitude of a reflection with contributions from both domains is

$$|F_{\rm tot}|^2 = k_1|F_1|^2 + k_2|F_2|^2, \qquad (1)$$

where $k_1/(k_1 + k_2)$ is the volume fraction of domain 1. More generally, if S independent domains with different structures, space-group symmetries and conventional unit cells can be referred to the same lattice base, all reflections are part of an apparently single reciprocal lattice. The corresponding Lp-corrected intensity on a relative scale is then

$$|F_{\rm tot}(\mathbf{h})|^2 = \sum_{s=1}^{S} k_s c_s(\mathbf{R}_s\mathbf{h})|F_s(\mathbf{R}_s\mathbf{h})|^2, \qquad (2)$$

where $|F_s|$ is the structure amplitude of structure s, k_s is the corresponding scaling factor, the matrix R_s transforms the indices h referred to the lattice base common to all structures into the conventional unit cell of structure s, and c_s is 1 if structure s contributes to the reflection and 0 if it does not. The volume ratios v_s of the domains are obtained from

$$v_s = (k_s V_s^2)/\left(\sum_{s=1}^{S} k_s V_s^2\right), \qquad (3)$$

where V_s are the volumes of the conventional unit cells. These formulae have been implemented in the program *STACK* (Birkedal *et al.*, 1998).

The starting parameters for refinement with *STACK* were taken from the interpretation in terms of the MDOs of the average structure obtained by direct methods. During the first cycles, the Hg—I distances were restrained to 2.7 Å since several parameters of different structures were highly correlated. In subsequent cycles, these restraints could be discarded and the refinement including anisotropic displacement parameters for all atoms converged to satisfactory reliability factors (Table 4). The atomic coordinates and anisotropic displacement parameters are given in Tables 5 and 6, respectively.

Table 5
Atomic coordinates refined with program *STACK*.

First line: MDO1, domain with space group $I4_1/amd$, origin at $2/m$, $a = 8.7863\,(5)$, $c = 24.667\,(3)$ Å. Second line: MDO2, domain with space group $P4_2/nmc$, origin at $\bar{1}$, lattice constants a and $c/2$. Third line: average layer with symmetry $p\bar{4}m2$, translation a and thickness $c/4$. The Wyckoff symbols refer to the respective space groups and for the third line to $P\bar{4}m2$. Line 3 is obtained from lines 1 and 2 through the respective transformations $x' = x - 0.5$, $y' = y - 0.25$, $z' = 4z - 0.5$ and $x' = x - 0.25$, $y' = y - 0.75$, $z' = 2z - 0.5$.

	Site	x	y	z	$U_{\rm eq}$
Hg	16 *h* .*m*.	0.74792 (15)	0.25	0.06232 (1)	0.0315 (2)
	8 *g* .*m*.	0.50043 (19)	0.75	0.12481 (13)	0.0399 (5)
	4 *j* .*m*.	0.24918	0.0	−0.25055	
I1	8 *e* 2*mm*.	0.5	0.75	0.25752 (9)	0.0249 (6)
	4 *d* 2*mm*.	0.25	0.25	0.5165 (3)	0.0343 (10)
	2 *g* 2*mm*.	0.0	0.5	0.5315	
I2	16 *g* ..2	0.76416 (14)	0.51416 (14)	0.125	0.0331 (3)
	8 *f* ..2	0.51381 (17)	0.01381 (17)	0.25	0.0292 (4)
	4 *h* ..2	0.26398	0.26398	0.0	
I3	8 *e* 2*mm*.	0.5	0.25	0.25758 (12)	0.0333 (7)
	4 *c* 2*mm*.	0.25	0.75	0.5136 (3)	0.0316 (9)
	2 *e* 2*mm*.	0.0	0.0	0.5288	

3.5. Determination of stacking probabilities from diffuse intensities

We now calculate the intensities $I(l)$ of the diffuse rods along the lattice rows with $h + k = 2n + 1$; the index l refers to the translation c of Tables 2 and 5 (thickness of four layers). A single layer of supertetrahedra is defined by the average atomic coordinates and anisotropic displacement parameters of MDO1 and MDO2 (third lines of Tables 5 and 6 with $z' = z/4$). The temperature difference between the Bragg data set and the diffuse profiles is neglected. The theory for the idealized structure was presented by S69. In Appendix *A*, we derive the formulae applicable to the present more general case and also correct an erroneous expression of S69.

Two successive layers of supertetrahedra may assume two types of relative positions, designated by *f* and *t* (Fig. 5 and §3.2). A single layer of supertetrahedra is delimited by the horizontal edges perpendicular to *c* formed by I1 and I3

Table 6
Anisotropic displacement parameters refined with program *STACK*.

For explanations, see Table 5. The displacement factor expression is $\exp(-2\pi^2 \sum U^{ij} a_i^* a_j^* h_i h_j)$.

	U^{11}	U^{22}	U^{33}	U^{12}	U^{13}	U^{23}
Hg	0.0266 (4)	0.0360 (4)	0.0318 (2)	0.0	0.0003 (3)	0.0
	0.0367 (7)	0.0446 (7)	0.0385 (11)	0.0	−0.0008 (3)	0.0
	0.0317	0.0403	0.0352	0.0	−0.0003	0.0
I1	0.0304 (11)	0.0261 (10)	0.0182 (9)	0.0	0.0	0.0
	0.058 (2)	0.0146 (13)	0.0301 (14)	0.0	0.0	0.0
	0.044	0.0204	0.0242	0.0	0.0	0.0
I2	0.0313 (4)	0.0313 (4)	0.0364 (6)	−0.0034 (4)	0.0001 (2)	−0.0001 (2)
	0.0302 (7)	0.0302 (7)	0.0272 (8)	−0.0029 (5)	0.0008 (3)	−0.0008 (3)
	0.0308	0.0308	0.0318	−0.0032	0.0005	−0.0005
I3	0.0335 (12)	0.0355 (12)	0.0308 (12)	0.0	0.0	0.0
	0.0454 (18)	0.0282 (16)	0.0211 (14)	0.0	0.0	0.0
	0.0395	0.0319	0.0260	0.0	0.0	0.0

(Fig. 6). The upper edges of a layer and the lower edges of the neighboring layer along $+c$ form together a slightly corrugated square net. These layer contacts are very similar for *f* and *t* stacks. They would be completely identical if the *z* coordinates and the displacement parameters of I1 and I3 assumed exactly the same values. This close similarity of the interface between layers explains the polytypic disorder. The I2 and Hg atoms of different layers are not in direct contact and are indeed disposed quite differently in *f* and *t* stacks. The simplest model assumes that the relative positions of any two distant layers depends only on the probabilities ω and $1-\omega$ of finding a *t* or an *f* stack, respectively. This model produces maxima of $I(l)$ at $l = 2n+1$ for $\omega < 1/2$ or at $l = 2n$ for $\omega > 1/2$, *i.e.* essentially MDO1 or MDO2, but never a mixture of both MDOs as observed. At least two probabilities must be postulated to obtain maxima of $I(l)$ at all integral values of l: ω_1 that a layer be *t* stacked on an *f* stack, and ω_2 that a layer be *t* stacked on a *t* stack:

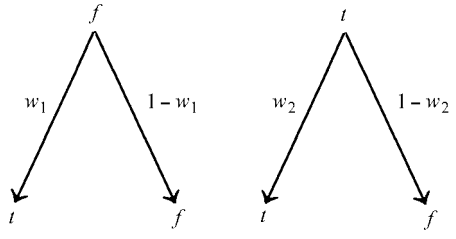

Equations (6) and (9) of Appendix *A* represent the rods of diffuse intensity $I(l)$ for this model in closed form. The average thickness of pure domains is $d_{\rm MDO1} = 1/\omega_1$ and $d_{\rm MDO2} = 1/(1-\omega_2)$, respectively. The corresponding fraction of pure domains thicker than *N* layers is $q_{\rm MDO1} = (1-\omega_1)^N$ and $q_{\rm MDO2} = \omega_2^N$.

The observed intensity $O(l)$ is a convolution of $I(l)$ with a Gaussian function whose variance depends on the divergence of the incident beam and the resolution of the detector. The scale factor *k*, the square root of the variance δl, and the probabilities ω_1 and ω_2 have been adjusted visually to several observed intensity profiles with different *h* and *k* values. The results are shown in Fig. 7. Small variations by 0.02 of ω_1 or ω_2 induce noticable deviations from the experimental profiles. This strong power of discrimination allow us to estimate the best set of probabilities with rather small uncertainties, $\omega_1 = 0.19\,(1)$ and $\omega_2 = 0.80\,(1)$. This gives an average thickness of pure domains $d_{\rm MDO1} = 5.3$ and $d_{\rm MDO2} = 5.0$ layers. The fraction of pure domains thicker than *N* layers is $q_{\rm MDO1} = 0.81^N$ and $q_{\rm MDO2} = 0.80^N$. We note that diffuse rods could in principle also arise for *h* and *k* both odd. However, the corresponding structure factors are very small (see Appendix *A*), and no such intensities have been observed experimentally. Appendix *A* also presents an alternative fit to the observations with $\omega_1 \simeq 0.80$ and $\omega_2 \simeq 0.20$, which corresponds to a twinned disordered *ftft*... structure. We rule this model out because S69 observed pure MDO1 crystals.

4. Conclusions

The quantitative interpretation of the diffraction patterns of polytypic orange HgI_2 confirms the qualitative results of S69: the structures are indeed stacking variants of layers of corner-linked Hg_4I_{10} supertetrahedra, which are fractal versions of the layers of tetrahedra found in the stable red form. The precision of the structure determination now permits us to make a detailed comparison of the bond lengths with those found in the red form and to discuss the interface between the layers.

There are three different Hg—I bond lengths (Table 7) that deviate by 0.01 Å (5 s.u.) from their average. The longest one is to a corner, the others to the mid-edges of the supertetrahedron. The edge oblique to *c* associated with the intermediate Hg—I bond is slightly bent, I1—I2—I1 = 175.68 (1)°, whereas the edge perpendicular to *c* corresponding to the shortest Hg—I bond is nearly straight, I1—I3—I1 =

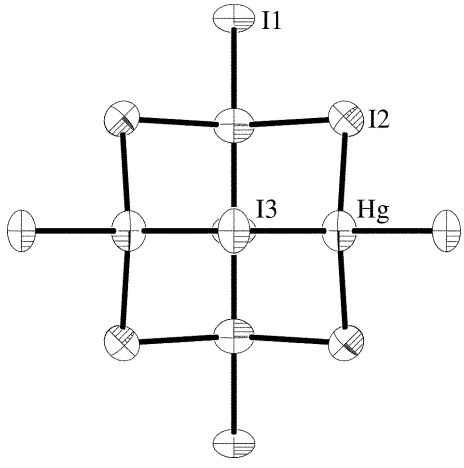

Figure 6
Supertetrahedra Hg_4I_{10} of the MDO1 structure viewed along the *c* axis, symmetry $\bar{4}2m$. The atomic displacement parameters are drawn at the 80% probability level.

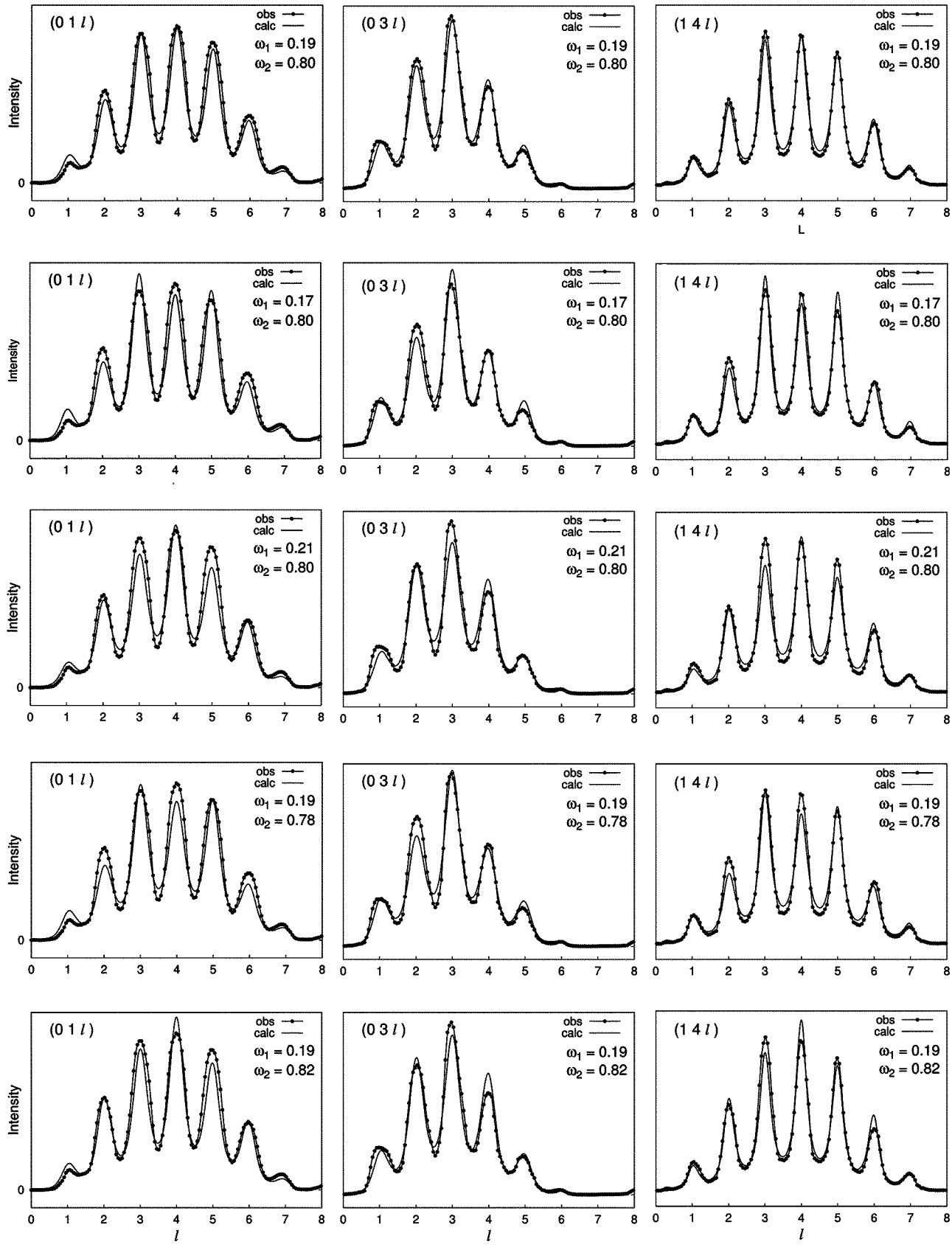

Figure 7
Profiles of diffuse intensity: left (01l); middle (03l); right (14l). Experimental profiles are drawn with dotted lines, calculated ones with full lines. Five different sets of probabilities are given. The best set is $\omega_1 = 0.19$, $\omega_2 = 0.80$ (first line). Square roots of the variances of the Gaussian function are $\delta l = 0.0045$, 0.0040 and 0.0180 for (01l), (03l) and (14l), respectively.

Table 7
Distances (Å) using the average layer geometry; s.u.values in parentheses.

Maximal deviations from the two refined structures MDO1 and MDO2 are less than 0.004 Å for Hg—I and less than 0.01 Å for I—I. Codes for supertetrahedron: *c* corner; *m* mid-edge; *E* aligned with edge; *e* oblique to edge; *l* contact between supertetrahedra in the same layer. Codes for contacts between different layers: v_1 perpendicular to *c* axis; v_2 oblique to *c* axis.

Supertetrahedron			Contacts MDO1		Contacts MDO2		
Hg—I1	2.801 (3)	*c*					
Hg—I2	2.788 (2)	*m*					
Hg—I3	2.776 (2)	*m*					
I1—I3	4.393 (2)	*E*	I1—I1	4.409 (1)	I1—I3	4.408 (1)	v_1
I1—I2	4.515 (3)	*E*	I3—I3	4.406 (1)	I3—I1	4.408 (1)	v_1
I2—I3	4.618 (3)	*e*	I1—I2	4.123 (2)	I2—I3	4.136 (2)	v_2
I2—I2	4.634 (3)	*e*	I2—I3	4.262 (2)	I1—I2	4.249 (2)	v_2
I2—I2	4.152 (3)	*l*					

179.53 (1)°. The average Hg—I bond length of 2.788 Å is nearly the same as the bond length of 2.786 (3) Å in the red form.[2]

The I—I contacts in the orange and red forms are also very similar: *E*, *e* and $l + v_2$ in Table 7 correspond in the red form to the distances 4.361 (3) Å, 4.641 (3) Å and 4.136 (3) Å, respectively. The layers of supertetrahedra interpenetrate by 0.36 Å; the strings of atoms I1 and I3 in the interface thus form a slightly undulating and nearly square net with an edge length of 4.4 Å. The contacts between the layers v_1 and v_2 are very similar in MDO1 and MDO2. They would be identical for equal *z* coordinates and displacement parameters of I1 and I3. It is these nearly identical contacts that lead to the stacking disorder. In a classical polytypic structure, pairs of adjacent layers are identical for several layer positions, *e.g.* *AB* and *AC* in a closest-sphere packing (Dornberger-Schiff, 1979). In orange HgI_2, however, stackings of adjacent layers differ for *f* and *t* (Fig. 5), and only the contacts are identical. The stacking variants thus possess the same slightly distorted cubic closest packing of I atoms and differ only by the distribution of Hg atoms in tetrahedral interstices. The anisotropic displacement parameters of Hg and I2 atoms are more spherical than those of I1 and I3 (Table 6, Fig. 6). The largest r.m.s. amplitudes of I1 and I3 are perpendicular to the I—I edges on the layer surface, whereas the Hg and I2 atoms are located inside the layer. The supertetrahedron may thus be a relatively rigid entity.

The probabilities ω_2 and $1 - \omega_1$ assume nearly the same value of about 0.8. This result gives a volume ratio of 50.6 (12)% for the MDO1 structure, which differs from the value of 59.5 (13)% obtained with *STACK*. This disagreement of about 9% corresponds to 7 s.u. and may be due to the approximations inherent in the measurement and refinement procedure of *STACK*. It may be difficult to properly attribute the intensities on the diffuse rods to the reciprocal lattice points: if some reflection profiles associated with the stacking sequence MDO2 are slightly broader than those from MDO1, their integrated intensities will be underestimated by a few percent. It is noteworthy that ω_2 and $1 - \omega_1$ assume nearly equal values. This near equality might indicate that the stacking sequences of MDO1 and MDO2 have roughly the same stability but are somewhat more stable than mixed stackings *ft* and *tf*. The average domain size is 30–32 Å, and 50% of the ordered stacks are thicker than four layers. Note that S69 described diffraction patterns of MDO1 crystals where the reflections of MDO2 were not observed. MDO1 and MDO2 should be described as two different, albeit closely related, structures. In Hostettler & Schwarzenbach (2002), we show that the orange phase in fact comprises three different structures. In view of their close resemblance, we have decided to refer to a single orange phase and to distinguish between the terms *structure* and *phase*.

[2] Distances calculated from the structural parameters reported by Jeffrey & Vlasse (1967).

APPENDIX *A*
Calculation of the rods of diffuse intensity

The derivation of the diffuse intensities as functions of the continuous index *L* along the rods *hkL* with $h + k = 2n + 1$ follows S69 closely. We use here exactly the same nomenclature as S69, and present details only where the present derivation differs from S69. The index $L = l/4$ refers to the separation of adjacent layers, $c/4 = 6.1668\,(8)$ Å, and *l* refers to the translation *c* used in the refinement of the MDO structures (Table 5).

The stacking of adjacent layers in MDO1 is denoted by the letter *f* (from four-layer structure); in MDO2 it is denoted by *t* (from two-layer structure). The layer positions with respect to the tetragonal *a* and *b* axes are denoted by the capital letters *A*, *B*, *C*, *D* and by the Greek letters α, β, γ, δ. When moving along the +*c* axis, layers adjacent to *A* are either *B* (*f* stack) or β (*t* stack); α may be followed either by δ (*f*) or by *D* (*t*). The admissible nearest neighbors of the other layers are obtained by cyclic permutations of the letters. The center of the Hg_4I_{10} supertetrahedron of layer *A* is placed at the origin 0, 0, 0. The atomic coordinates and displacement factors are then those given in Tables 5 and 6 for the average layer. Layers α, γ and *C* are shifted relative to *A* by *a*/2, *b*/2 and $(a + b)/2$, respectively. Layers δ, *B*, *D* and β are obtained by inversion of *A* at the origin and displacements of 0, *a*/2, *b*/2 and $(a + b)/2$, respectively. The intensity $I(L)$ along the lattice row *hkL* is given by (Wilson, 1942; Jagodzinski, 1954)

$$I(L) = \sum_{m=-(N-1)}^{N-1} (N - |m|)\, J_m \exp(-2\pi i L m); \qquad (4)$$

$$J_m = \sum_r \sum_s p_r\, P_{rs}^{(m)}\, F_r\, F_s^*. \qquad (5)$$

N is the number of layers; p_r is the *a priori* probability of finding in the stack a layer of type *r*; $P_{rs}^{(m)}$ is the *a posteriori* probability of finding a layer of type *s*, *m* layers from one of type *r*; and F_r is the structure factor of the layer of type *r*. The derivation supposes that all layer types occur with equal probability and that on average all layers are equivalent. Thus, $p_r = 1/8$ for all *r*, and there remain only eight types of probabilities $P_{As}^{(m)}$, with $s = A$, α, *C* or γ for *m* even and $s = B$, β, *D* or δ for *m* odd. These conditions are sufficient to ensure

tetragonal symmetry $p\bar{4}m2$ for an average layer and a tetragonal diffraction pattern. Probabilities for m odd are determined by probabilities for m even, since layer types B and β are always stacked along $+c$ on layer types A and γ; D and δ on C and α; A and α on D and β; and C and γ on B and δ. Thus

$$P_{AB}^{(2n+1)} + P_{A\beta}^{(2n+1)} = P_{AA}^{(2n)} + P_{A\gamma}^{(2n)},$$

$$P_{AD}^{(2n+1)} + P_{A\delta}^{(2n+1)} = P_{AC}^{(2n)} + P_{A\alpha}^{(2n)},$$

$$P_{AA}^{(2n)} + P_{A\alpha}^{(2n)} = P_{AD}^{(2n-1)} + P_{A\beta}^{(2n-1)},$$

$$P_{AC}^{(2n)} + P_{A\gamma}^{(2n)} = P_{AB}^{(2n-1)} + P_{A\delta}^{(2n-1)}.$$

Going from m to $-m$ we have $P_{rs}^{(-m)} = P_{sr}^{(m)}$. In particular, from $P_{AB}^{(-2n+1)} + P_{A\beta}^{(-2n+1)} = P_{AA}^{(-2n)} + P_{A\gamma}^{(-2n)}$ we get

$$\begin{aligned} P_{BA}^{(2n-1)} + P_{\beta A}^{(2n-1)} &= P_{AD}^{(2n-1)} + P_{A\beta}^{(2n-1)} = P_{AA}^{(2n)} + P_{\gamma A}^{(2n)} \\ &= P_{AA}^{(2n)} + P_{A\gamma}^{(2n)}, \end{aligned}$$

whence $P_{A\alpha}^{(2n)} = P_{A\gamma}^{(2n)}$.

S69 assumed an idealized structure, where only the Hg atoms contribute to the diffuse intensities. We now must include in the structure factor of layer A, $F_A(hkL) = a_{hkL} + ib_{hkL}$, all atoms of the average layer (Table 5) with the corresponding anisotropic displacement parameters (Table 6). Following in all other respects S69, we obtain the following for the intensity distribution $I(L)$ for $h + k = 2n + 1$ instead of equation (6) of S69:

$$I(L) = 2N\left[a_{hkL}\sin(\pi L) + (-1)^h b_{hkL}\cos(\pi L)\right]^2 S(L), \qquad (6)$$

$$S(L) = \left[1 + 2\sum_{n=1}^{\infty}(P_{AA}^{2n} - P_{AC}^{2n})\cos(4\pi Ln)\right].$$

In order to calculate the stacking interference function $S(L)$, we now express, as in S69, $P_{AA}^{(2n)} - P_{AC}^{(2n)}$ as functions of the nearest-neighbor probabilities ω_1 for an f stack to be followed by a t stack and ω_2 for a t stack to be followed by a t stack; $1 - \omega_1$ and $1 - \omega_2$ are the corresponding probabilities for an f stack to be followed by an f stack and for a t stack to be followed by an f stack. Denoting by $a_1^{(m)}$ the probability that the mth layer has position A and is f stacked and by $a_2^{(m)}$ that it is t stacked, so that $a_1^{(m)} + a_2^{(m)} = P_{AA}^{(m)}$ $(m = 2n)$, and using analogous symbols for layers with position C, α and γ, the Markov chain relating probabilities of the layer $2n$ to those of the layer $2n - 2$ is easily written in matrix form:

$$\mathbf{p}^{(2n)} = \mathbf{P}\,\mathbf{p}^{(2n-2)} = \mathbf{P}^n\,\mathbf{p}^{(0)},$$

with $\mathbf{p}^{(2n)} = [a_1^{(2n)}\, a_2^{(2n)}\, c_1^{(2n)}\, c_2^{(2n)}\, \alpha_1^{(2n)}\, \alpha_2^{(2n)}\, \gamma_1^{(2n)}\, \gamma_2^{(2n)}]^T$ a column vector and $\mathbf{P}$ an 8×8 matrix. For calculating $P_{AA}^{(2n)} - P_{AC}^{(2n)}$, the matrix $\mathbf{P}$ can be compressed into the 2×2 matrix $\mathbf{M}$ given by S69. Defining the components of the two-vector $\mathbf{d}^{(2n)}$ by $d_i^{(2n)} = a_i^{(2n)} - c_i^{(2n)}$ $(i = 1, 2)$,

$$\mathbf{d}^{(2n)} = \mathbf{M}\mathbf{d}^{(2n-2)} = \mathbf{M}^n\mathbf{d}^{(0)}, \qquad (7)$$

$$P_{AA}^{(2n)} - P_{AC}^{(2n)} = d_1^{(2n)} + d_2^{(2n)},$$

$$\mathbf{M} = \begin{pmatrix} \omega_1(1-\omega_2) - (1-\omega_1)^2 & \omega_1(1-\omega_2) - (1-\omega_2)^2 \\ \omega_1^2 - \omega_1(1-\omega_2) & \omega_2^2 - \omega_1(1-\omega_2) \end{pmatrix},$$

$$\mathbf{d}^{(0)} = (1 - \omega_2 + \omega_1)^{-1}\begin{pmatrix} 1-\omega_2 \\ \omega_1 \end{pmatrix}.$$

The components of $\mathbf{d}^{(0)}$ are the probabilities $a_1^{(0)}$ for finding an f stacking in the crystal and $a_2^{(0)}$ for finding a t stacking. The determinant of $\mathbf{M}$ is $|\mathbf{M}| = (\omega_1 - \omega_2)^2$. Equation (6) can be evaluated without attempting to explicitly obtain $\mathbf{M}^n$ [equation (10) of S69 is incorrect]. An explicit expression for $S(L)$ is obtained by summing a series of 2×2 matrices:

$$\begin{aligned} \mathbf{s} &= \sum_{n=0}^{\infty}\mathbf{d}^{(2n)}\exp(4\pi iLn) = \left[\sum_{n=0}^{\infty}\mathbf{M}^n\exp(4\pi iLn)\right]\mathbf{d}^{(0)} \\ &= [\mathbf{1} - \mathbf{M}\exp(4\pi iL)]^{-1}\mathbf{d}^{(0)}, \end{aligned} \qquad (8)$$

where $\mathbf{s}$ is a two-vector, $\mathbf{1}$ is the 2×2 unit matrix, and the matrix at the right is always invertible except in some limiting cases of ordered structures with ω_1 and ω_2 equal to 0 or 1. The interference function $S(L)$ in (6) is then obtained by summing the components of $\mathbf{s}$ and taking the real part,

$$\begin{aligned} S(L) &= 2\mathrm{Re}(s_1 + s_2) - 1 \\ &= T/\left[U + V\sin^2(2\pi L) + W\sin^2(4\pi L)\right], \end{aligned} \qquad (9)$$

with

$$T = \omega_1(1-\omega_2)[1 - (\omega_1 - \omega_2)^4],$$

$$U = (1-\omega_2)^2[1 - (\omega_1 - \omega_2)^2]^2,$$

$$V = [\omega_1^2 - (1-\omega_2)^2][1 - (\omega_1 - \omega_2)^2]^2,$$

$$W = (\omega_1 - \omega_2)^2(1 + \omega_1 - \omega_2)^2.$$

$S(L)$ reduces to S69's equation (9) for $\omega = \omega_1 = \omega_2$, which shows maxima at $L = 1/4$, 3/4 for $\omega < 0.5$ or at $L = 0$, 1/2 for $\omega > 0.5$, corresponding, respectively, to disordered MDO1 and MDO2. For $\omega_1 = \omega$, $\omega_2 = 1 - \omega$, (9) reduces to

$$S(L) = (1 - \nu^2)/[(1-\nu)^2 + 4\nu\sin^2(4\pi L)], \qquad (10)$$

with $\nu = (1 - 2\omega)^2$. Equation (10) shows maxima at both $L = 0$, 1/2 and $L = 1/4$, 3/4, as experimentally observed. Interestingly, $S(L)$ assumes identical values for ω and $1 - \omega$, although the corresponding stackings are not identical. For $\omega > 0.5$, f tends to be followed by t, and t by f; in the limit of $\omega \to 1$, we have twinned domains of an ordered orthorhombic (*Amma*) structure $ftft\ldots + tftf\ldots$. For $\omega < 0.5$, we have domains of disordered MDO structures; in the limit of $\omega \to 0$, we approach the model refined with the program *STACK*, $fff\ldots + ttt\ldots$.

Along the lattice lines with both h and k odd, there are, in theory, also diffuse rods whose calculated intensities are products analogous to (6) of effective structure factors and stacking interference functions $S_e(L)$ for even intervals between layers [$m = 2n$ in (4) and (5)] and $S_o(L)$ for odd intervals $(m = 2n + 1)$,

$$I(L) = (a_{hkL}^2 + b_{hkL}^2)S_e(L) + (a_{hkL}^2 - b_{hkL}^2)S_o(L). \qquad (11)$$

It is possible, but very laborious, to obtain an explicit expression for $S_e(L)$ and $S_o(L)$ as functions of ω_1 and ω_2 using the methods presented above. However, no intensities have been observed experimentally for h and k odd. Indeed, both a_{hkL} and b_{hkL} are very small quantities. They compute to exactly zero under the following conditions:

$$x(\mathrm{Hg}) = 1/4, \quad z(\mathrm{I1}) = z(\mathrm{I3}), \quad x(\mathrm{I2}) = 1/4;$$

$$U^{12} = U^{13} = U^{23} = 0 \text{ for Hg and I2},$$

$$U^{11}(\mathrm{I1}) = U^{11}(\mathrm{I3}), \quad U^{22}(\mathrm{I1}) = U^{22}(\mathrm{I3}), \quad U^{33}(\mathrm{I1}) = U^{33}(\mathrm{I3}).$$

These conditions are reasonably well obeyed in the average layer, the largest deviation of the real structure being due to I2. Its contribution to the effective structure factor is

$$a_{hkL}^2 = \left\{4f(I)\,\sin[2\pi h(x-1/4)]\,\sin[2\pi k(x-1/4)]\right\}^2,$$

$$x - 1/4 = 0.0137,$$

which is always small compared with the observed intensities. We thus arrive at the interesting conclusion that stacks $ftft\ldots + tftf\ldots$ (*e.g.* $AB\gamma\beta$ and $A\beta\alpha D$) and alternating stacks of MDO structures with equal volumes $fff\ldots + ttt\ldots$ are strictly indistinguishable for an idealized layer, and indistinguishable in practice. Single untwinned crystals would, of course, always be distinguishable.

We thank the Swiss National Science Foundation for financial support. HB acknowledges financial support from the Danish Research Training Council and the Danish Natural Science Research Council.

References

Bernstein, J., Davey, R. J. & Henck, J.-O. (1999). *Angew. Chem. Int. Ed. Eng.* **38**, 3440–3461.
Bijvoet, J. M., Claasen, A. & Karssen, A. (1926). *Proc. Acad. Sci. Amst.* **29**, 529–546.
Birkedal, H., Hostettler, M., Schwarzenbach, D. & Paciorek, W. (1998). *Bull. Czech Slovak Cryst. Assoc.* **5**, 200.
Bube, R. H. (1957). *Phys. Rev.* **106**, 703–715.
Dornberger-Schiff, K. (1979). *Krist. Tech.* **14**, 1027–1045.
Gorskii, V. S. (1934). *Phys. Z. Sowjet*, **6**, 515.
Gorskii, V. S. (1935). *J. Exp. Theoret. Phys. USSR*, **5**, 155–158. (In Russian.)
Gumiński, C. (1997). *J. Phase Equil.* **18**, 206–215.
Hostettler, M. (2002). PhD thesis, Université de Lausanne, Switzerland.
Hostettler, M., Birkedal, H. & Schwarzenbach, D. (2001). *Chimia*, **55**, 541–545.
Hostettler, M. & Schwarzenbach, D. (2002). *Acta Cryst.* B**58**, 914–920.
IGOR (2000). *IGOR Pro.* Version 4.0. WaveMetrics Inc., Oregon, USA.
Jagodzinski, H. (1954). *Acta Cryst.* **7**, 17–25.
Jeffrey, G. A. & Vlasse, M. (1967). *Inorg. Chem.* **6**, 396–399.
Kim, J. & Hughbanks, T. (2000). *J. Solid State Chem.* **149**, 242–251.
Kleber, W., Raidt, H. & Leupold, K. O. (1968). *Krist. Tech.* **3**, 65–78.
Kohlschütter, H. W. (1927). *Kolloidchem. Beih.* **24**, 319–364.
Lehmann, M. S. & Larsen, F. K. (1974). *Acta Cryst.* A**30**, 580–584.
Oxford Diffraction (2001). Xcalibur System, User Manual. *CrysAlis* Software Package. Version 1.167. Oxfordshire, UK.
Piechotka, M. (1997). *Mater. Sci. Eng.* **18**, 1–98.
Schieber, M., Hermon, H., Vilensky, A., Melekhov, L., Shatunovsky, R., Meerson, E. & Saado, H. (2001). *Nucl. Inst. Methods Phys. Res. A*, **458**, 41–46.
Schwarzenbach, D. (1969). *Z. Kristallogr.* **128**, 97–114.
Sharma, S. L., Pal, T. & Acharya, H. N. (1994). *J. Appl. Phys.* **75**, 7884–7893.
Sheldrick, G. M. (1997). *SHELXS*97. University of Göttingen, Germany.
Steiner, B., van den Berg, L. & Laor, U. (1999). *J. Appl. Phys.* **86**, 4677–4687.
Stoe & Cie GmbH (1997). *IPDS* 2.87 Software Manual. Darmstadt, Germany.
Trigunayat, G. C. (1966). *Nature* (*London*), **19**, 808–809.
Trigunayat, G. C. & Verma, A. R. (1962). *Acta Cryst.* **15**, 499–504.
Vannerberg, N.-G. (1970). *Structure Reports*, Vol. 34A, edited by W. B. Pearson, p. 182. Chester, UK: International Union of Crystallography.
Wilson, A. J. C. (1942). *Proc. R. Soc. London Ser. A*, **180**, 277–285.
XPREP (1996). *XPREP.* Version 5.04. Siemens Analytical X-ray Instruments, Madison, Wisconsin, USA.